Direct numerical simulation of an arbitrarily shaped particle at a fluidic interface

Lecrivain, G.; Yamamoto, R.; Hampel, U.; Taniguchi, T.;

Originally published:

June 2017

Physical Review E 95(2017), 063107

DOI: https://doi.org/10.1103/PhysRevE.95.063107

Direct numerical simulation of an arbitrarily shaped particle at a fluidic interface

Gregory Lecrivain,[1,2,*] Ryoichi Yamamoto,[1] Uwe Hampel,[2,3] and Takashi Taniguchi[1,†]

[1] *Kyoto University, Department of Chemical Engineering, Kyoto 615-8510, Japan*
[2] *Helmholtz-Zentrum Dresden-Rossendorf, Institut für Fluiddynamik, Bautzner Landstraße 400, 01328 Dresden, Germany*
[3] *Technische Universität Dresden, AREVA-Stiftungsprofessur für Bildgebende Messverfahren für die Energie- und Verfahrenstechnik, 01062 Dresden, Germany*

(Dated: May 30, 2017)

A consistent formulation is presented for the direct numerical simulation of an arbitrarily shaped colloidal particle at a deformable fluidic interface. The rigid colloidal particle is decomposed into a collection of solid spherical beads and the three-phase boundaries are replaced with smoothly spreading interfaces. The major merit of the present formulation lies in the ease, with which the geometrical decomposition of the colloidal particle is implemented, yet allowing the dynamic simulation of intricate three-dimensional colloidal shapes in a binary fluid. The dynamics of a rod-like, of a plate-like, and of a ring-like particle are presently tested. It is found that plate-like particles attach more rapidly to a fluidic interface and are subsequently harder to dislodge when subject to an external force. Using the Bond number, i.e. the ratio of the gravitational force to the reference capillary force, a spherical particle with equal affinity for the two fluids breaks away from a fluidic interface at the critical value Bo = 0.75. This value is in line with our numerical experiments. It is here shown that a plate and a ring of equivalent masses detach at greater critical Bond numbers approximately equal to Bo = 1.3. Results of this study will find applications in the stabilisation of emulsions by colloids and in the recovery of colloidal particles by rising bubbles.

I. INTRODUCTION

Solid particles of colloidal dimensions, which adsorb at a fluidic interface, are present in a wide range of applications. Notable examples include the stabilisation of emulsions [1] and the recovery of minerals by rising bubbles [2]. The growing interest in the fundamental understanding of these processes has motivated us to develop a fully-resolved three dimensional model. The majority of the existing three-phase flow models found in the literature is restricted to simple colloidal shapes, for which a precise mathematical representation exists. The bulk of these numerical advancements have largely involved spheres [3, 4] and only a handful have considered ellipsoidal particles [5–7]. When it comes to arbitrarily shaped colloids mostly two-dimensional studies are found in the literature [8, 9]. The scarcity of three-dimensional extensions can probably be attributed to the difficulty in representing the particle shape and to the associated higher computational cost [10]. The decomposition of an arbitrarily shaped colloidal particle into a collection of spherical beads is here suggested. While the idea behind such a geometrical decomposition has already been suggested in the past [11], we are the first to report a consistent formulation with realistic three dimensional applications. Our new formulation applies to the category of so-called "diffuse interface models", meaning that each phase boundary is replaced with a smoothly spreading interface [8, 9, 12–14]. The major merit of the present formulation lies in the ease, with which the representation of the intricate three-dimensional shape of the colloid is implemented. Another advantage is the effective simulation of the inter-particle interactions in a system made of multiple arbitrarily shaped colloids. The dynamics of a rod-like, of a plate-like, and of a ring-like particle at a fluidic interface are presently tested.

* g.lecrivain@hzdr.de
† taniguch@cheme.kyoto-u.ac.jp

II. MODEL

A. Representation of the solid assembly

The arbitrarily shaped rigid colloid, hereafter referred to as the *solid assembly*, is decomposed into a collection of N_b spherical beads. To numerically represent the three-dimensional shape of the b-th bead the volume fraction $\phi_b(\mathbf{x},t)$ is introduced. As one moves from the inner bead to the outer bead region the volume fraction ϕ_b smoothly transitions from unity to zero across a diffuse interface of length ξ_b. A number of smooth profiles are suggested in reference [15]. We here use a truncated hyperbolic function defined as

$$\phi_b(\mathbf{x}) = \begin{cases} 1 & \text{if } |\boldsymbol{\ell}_b| < \mathrm{r}_b - \xi_c, \\ 0 & \text{if } |\boldsymbol{\ell}_b| > \mathrm{r}_b + \xi_c, \\ \frac{1}{2}\left[\tanh\left(\frac{\mathrm{r}_b - |\boldsymbol{\ell}_b|}{\xi_b/2}\right) + 1\right] & \text{else.} \end{cases} \tag{1}$$

where r_b is the bead radius, $\boldsymbol{\ell}_b(\mathbf{x}) = \mathbf{x} - \mathbf{X}_b$ the distance vector from the bead centre of mass $\mathbf{X}_b$ to the spacial coordinate $\mathbf{x}$, and ξ_c a cut-off length. Introducing capital letters to distinguish between the Lagrangian and the Eulerian fields, the volume fraction of the solid assembly

"S" is suggested as

$$\phi_{\mathrm{S}}(\mathbf{x}) = \frac{\sum\limits_{b\in \mathrm{S}} \phi_b(\mathbf{x})}{\max\left[\sum\limits_{b\in \mathrm{S}} \phi_b(\mathbf{x}), 1\right]}. \tag{2}$$

Note that the capital letter "S" differentiates the field ϕ_{S} of the "Solid" assembly from the field ϕ_b of the b-th spherical "bead". The denominator in Equation (2), originally suggested by Molina and Yamamoto [16], ensures that the total volume fraction ϕ_{S} remains lower than unity when the smooth profiles of several neighbouring beads overlap. Note that the truncation is used primarily to speed up the execution time since the hyperbolic function is only calculated across the diffuse interface of the colloid. The effect of the truncation on the drag force is discussed in the result section. Its effect on the contact angle is discussed in the reference [14]. A significant advantage of the present representation lies in the ease with which the implementation of ϕ_{S} is done, yet allowing a large freedom in describing the three dimensional shape of the assembly.

B. Transport of the solid assembly

The centre of mass of the solid assembly is denoted by $\mathbf{X}_{\mathrm{S}} = (\mathrm{X_S}\,\mathrm{Y_S})^\top$, where the upperscript $^\top$ indicates the transpose operator. As illustrated in Figure 1 the position $\hat{\mathbf{X}}_b$ of the b-th spherical bead is fixed in the body frame, i.e. in the frame moving with the solid assembly. The hat symbol indicates a quantity expressed in the body frame. The bead position in the inertial frame is given by

$$\mathbf{X}_b = \mathbf{X}_{\mathrm{S}} + \mathbf{R}_{\mathrm{S}} \cdot \hat{\mathbf{X}}_b, \tag{3}$$

where $\mathbf{R}_{\mathrm{S}}$ is the rotation matrix associated with the solid assembly. The rotation matrix is expressed as a function of the four dimensional quaternion $\mathbf{Q}_{\mathrm{S}} = (q_0\, q_1\, q_2\, q_3)^\top$, where q_0 denotes the scalar part of the quaternion and $(q_1\, q_2\, q_3)^\top$ the three dimensional vector part. The rotation matrix is given by

$$\mathbf{R}_{\mathrm{S}} = 2\begin{pmatrix} \frac{1}{2} - q_2^2 - q_3^2 & q_1q_2 - q_0q_3 & q_1q_3 + q_0q_2 \\ q_1q_2 + q_0q_3 & \frac{1}{2} - q_1^2 - q_3^2 & q_2q_3 - q_0q_1 \\ q_1q_3 - q_0q_2 & q_2q_3 + q_0q_1 & \frac{1}{2} - q_1^2 - q_2^2 \end{pmatrix}. \tag{4}$$

For the computation of the time-dependent trajectory $\mathbf{X}_{\mathrm{S}}(t)$ of the solid assembly the hydrodynamic force $\mathbf{F}_h$, the capillary force $\mathbf{F}_c$, and an external force $\mathbf{F}_e$ representing the weight of the colloid are retained [14]. For readability purposes the Lagrangian transport equations are shown later in Equations (12-13, 16-17).

C. Fluidic interface model

In a similar fashion the fluidic boundary is replaced with a smoothly spreading interface layer. To this end

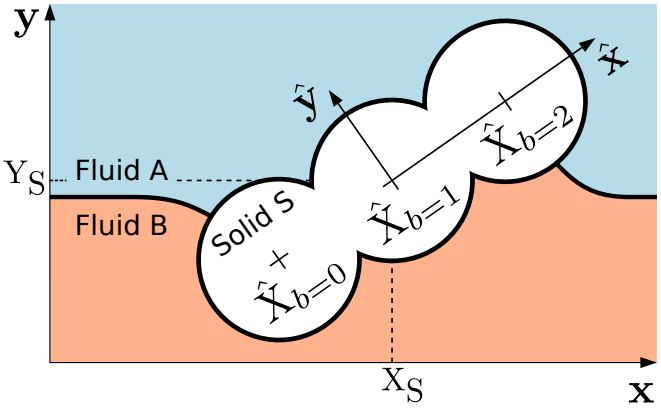

FIG. 1. Schematics of a solid assembly at a fluidic interface. The assembly is shown in the body frame and in the inertial frame.

the two additional volume fractions $\phi_{\mathrm{A}}(\mathbf{x}, t)$ and $\phi_{\mathrm{B}}(\mathbf{x}, t)$ respectively associated with the fluid "A" and the fluid "B" are introduced. The separation of the binary fluid mixture into its two constituent phases A and B is driven by the minimisation of the free energy

$$\mathcal{F} = \frac{k_{\mathrm{B}}T_0}{\mathrm{v}_0}\int_{\mathcal{V}} f(\phi_{\mathrm{A}}, \phi_{\mathrm{B}}, \phi_{\mathrm{S}})\mathrm{d}\mathbf{x} \tag{5}$$

where $\mathcal{V}$ is the region of space occupied by the isothermal system, k_{B} the Boltzmann constant, T_0 the temperature, v_0 a constant unit volume, and f the free energy density scaled by the reference energy density $\mu_0 = k_{\mathrm{B}}T_0/\mathrm{v}_0$. A number of formulations specifically developed for the use of diffuse interface models have been proposed [9, 12, 13]. The formulation recently suggested by the same authors and validated for a single sphere is here retained [14]. In their work, the free energy density was given by

$$\begin{aligned} f = f_{bulk} &+ \frac{\xi^2}{2}\left|\nabla(\phi_{\mathrm{A}} - \phi_{\mathrm{B}})\right|^2 \\ &+ \frac{\xi_{\mathrm{A}}^2}{2}\left|\nabla(\phi_{\mathrm{A}} - \phi_{\mathrm{S}})\right|^2 + \frac{\xi_{\mathrm{B}}^2}{2}\left|\nabla(\phi_{\mathrm{B}} - \phi_{\mathrm{S}})\right|^2 \end{aligned} \tag{6}$$

where $f_{bulk} = \phi_{\mathrm{A}}\ln(\phi_{\mathrm{A}}) + \phi_{\mathrm{B}}\ln(\phi_{\mathrm{B}}) + \chi\phi_{\mathrm{A}}\phi_{\mathrm{B}}$ was the bulk contribution and χ a parameter describing the affinity between the two fluid phases. The three tunable interfacial length scales ξ, ξ_{A}, and ξ_{B} preceding the gradient terms allowed for a change in the particle hydrophobicity. Because of the phase summation constraint $\phi_{\mathrm{A}} + \phi_{\mathrm{B}} + \phi_{\mathrm{S}} = 1$ the free energy is rewritten as $f(\psi, \phi_{\mathrm{S}})$, where this new order parameter is defined as $\psi(\mathbf{x}, t) = \phi_{\mathrm{A}} - \phi_{\mathrm{B}}$. This field ψ is updated in time according to the modified "Cahn-Hilliard" equation [13]

$$\frac{\partial\psi}{\partial t} + \nabla\cdot\left[\psi\mathbf{u} - M\left(\mathbf{I} - \mathbf{n}_{\mathrm{S}}\otimes\mathbf{n}_{\mathrm{S}}\right)\cdot\nabla\mu\right] = 0, \tag{7}$$

where M is the mobility, $\mathbf{I}$ the unit tensor, $\mathbf{n}_{\mathrm{S}} = -\nabla\phi_{\mathrm{S}}/|\nabla\phi_{\mathrm{S}}|$ the local unit vector normal to the surface of the solid assembly, and $\mu(\psi, \phi_{\mathrm{S}}) = \delta\mathcal{F}/\delta\psi$ the chemical potential. Away from the particle diffuse interface the outer product $\mathbf{n}_{\mathrm{S}}\otimes\mathbf{n}_{\mathrm{S}}$ is set to the zero tensor.

D. Coupling with hydrodynamics

The flow around the solid assembly is resolved using the "smooth profile method", which uses a fixed cartesian grid to solve the Navier-Stokes equations [15, 17]. The smooth profile method is particularly attractive to simulate the flow around moving objects since it suppresses the need for a remeshing algorithm. In this method the total fluid velocity field $\mathbf{u}$ is decomposed into two components as

$$\mathbf{u} = (1-\phi_{\mathrm{S}})\mathbf{u}_f + \phi_{\mathrm{S}}\mathbf{u}_{\mathrm{S}}. \tag{8}$$

The first term $(1-\phi_{\mathrm{S}})\mathbf{u}_f$ corresponds to the velocity field of the binary fluid. The second term is the velocity field of the solid assembly defined as

$$\phi_{\mathrm{S}}\mathbf{u}_{\mathrm{S}} = \phi_{\mathrm{S}}\left(\mathbf{V}_{\mathrm{S}} + \boldsymbol{\Omega}_{\mathrm{S}} \times \boldsymbol{\ell}_{\mathrm{S}}\right), \tag{9}$$

where $\mathbf{V}_{\mathrm{S}}$, $\boldsymbol{\Omega}_{\mathrm{S}}$, and $\boldsymbol{\ell}_{\mathrm{S}} = \mathbf{x} - \mathbf{X}_{\mathrm{S}}$ are respectively the translational velocity of the assembly, its rotational velocity, and the distance vector from the assembly centre of mass $\mathbf{X}_{\mathrm{S}}$. The evolution of the total field velocity, which satisfies the incompressibility condition $\nabla\cdot\mathbf{u}=0$ over the entire computational domain, is governed by the following modified momentum equation

$$\rho\left[\frac{\partial\mathbf{u}}{\partial t} + (\mathbf{u}\cdot\nabla)\,\mathbf{u}\right] = \nabla\cdot[-p\mathbf{I} + \boldsymbol{\sigma}_{\mathrm{v}}] - \psi\nabla\mu + \rho\phi_{\mathrm{S}}\mathbf{f}_{\mathrm{S}}, \tag{10}$$

where ρ is the density of the binary fluid, p the pressure, $\boldsymbol{\sigma}_{\mathrm{v}} = \eta[\nabla\mathbf{u} + (\nabla\mathbf{u})^{\top}]$ the viscous stress tensor, and η the viscosity. The first additional term $-\psi\nabla\mu$ is the capillary field with respect to the two fluid phases. The second additional term $\rho\phi_{\mathrm{S}}\mathbf{f}_{\mathrm{S}}$ is the penalty field, which enforces the rigidity constraint of the solid assembly. The development of the smooth profile method is now well documented and has found widespread applications ranging from the rheological behaviour of colloidal dispersion [18] to the study of self-propelled microorganisms [19]. Application of the smooth profile method to study the interaction of colloids with a binary fluid mixture, as is the case here, is however relatively new. For the sake of conciseness this section was intentionally kept short. Further reading on the smooth profile method may be found in the selected references [10, 15–17].

III. SIMULATION PROCEDURE

Let ψ^n be the order parameter at the initial time t^n. The field ψ^{n+1} is first advanced in time as

$$\psi^{n+1} = \psi^n - \int_{t^n}^{t^{n+1}} \nabla\cdot\mathbf{J}^n \mathrm{d}t,$$
$$\mathbf{J}^n = \psi^n\mathbf{u}^n - M\left(\mathbf{I} - \mathbf{n}_{\mathrm{S}}^n \otimes \mathbf{n}_{\mathrm{S}}^n\right)\cdot\nabla\mu^n. \tag{11}$$

The position of the centre of mass along with the quaternion of the solid assembly are then updated in time as

$$\mathbf{X}_{\mathrm{S}}^{n+1} = \mathbf{X}_{\mathrm{S}}^n + \int_{t^n}^{t^{n+1}} \mathbf{V}_{\mathrm{S}}^n \mathrm{d}t, \tag{12}$$

$$\mathbf{Q}_{\mathrm{S}}^{n+1} = \mathbf{Q}_{\mathrm{S}}^n + \frac{1}{2}\int_{t^n}^{t^{n+1}} \mathbf{A}_{\mathrm{S}}^n \cdot \mathbf{Q}_{\mathrm{S}}^n \mathrm{d}t. \tag{13}$$

The 4×4 orthogonal matrix $\mathbf{A}_{\mathrm{S}}$ is given by

$$\mathbf{A}_{\mathrm{S}} = \begin{pmatrix} 0 & -\Omega_x & -\Omega_y & -\Omega_z \\ \Omega_x & 0 & -\Omega_z & \Omega_y \\ \Omega_y & \Omega_z & 0 & -\Omega_x \\ \Omega_z & -\Omega_y & \Omega_x & 0 \end{pmatrix}, \tag{14}$$

where $(\Omega_x\,\Omega_y\,\Omega_z)^{\top} = \boldsymbol{\Omega}_{\mathrm{S}}$. A fractional step approach is employed to solve the momentum Equation (10). An intermediate velocity is first calculated as

$$\mathbf{u}^* = \mathbf{u}^n + \int_{t^n}^{t^{n+1}} \Big\{ -(\mathbf{u}^n\cdot\nabla)\,\mathbf{u}^n + \frac{1}{\rho}\Big[\nabla\cdot(-p^*\mathbf{I} + \boldsymbol{\sigma}_{\mathrm{v}}^n) - \psi^{n+1}\nabla\mu^{n+1}\Big]\Big\}\mathrm{d}t. \tag{15}$$

The intermediate pressure p^* is calculated by solving a Poisson equation $\nabla\cdot\mathbf{u}^* = 0$. The translational and rotational velocities of the solid assembly are updated in time as [20]

$$\mathbf{V}_{\mathrm{S}}^{n+1} = \mathbf{V}_{\mathrm{S}}^n + m_{\mathrm{S}}^{-1}\int_{t^n}^{t^{n+1}} \Big(\mathbf{F}_h + \mathbf{F}_c + \mathbf{F}_e\Big)\mathrm{d}t, \tag{16}$$

$$\hat{\boldsymbol{\Omega}}_{\mathrm{S}}^{n+1} = \hat{\boldsymbol{\Omega}}_{\mathrm{S}}^n + \hat{\mathbf{I}}_{\mathrm{S}}^{-1}\cdot\int_{t^n}^{t^{n+1}} \Big[-\hat{\boldsymbol{\Omega}}_{\mathrm{S}}^n \times \big(\hat{\mathbf{I}}_{\mathrm{S}}\cdot\hat{\boldsymbol{\Omega}}_{\mathrm{S}}^n\big) + \hat{\mathbf{T}}_h + \hat{\mathbf{T}}_c\Big]\,\mathrm{d}t \tag{17}$$

where $m_{\mathrm{S}} = \int \phi_{\mathrm{S}}\rho_{\mathrm{S}}\mathrm{d}\mathbf{x}$ is the mass of the solid assembly, $\mathbf{I}_{\mathrm{S}} = \int \phi_{\mathrm{S}}\rho_{\mathrm{S}}(\boldsymbol{\ell}_{\mathrm{S}}^2\mathbf{I} - \boldsymbol{\ell}_{\mathrm{S}}\otimes\boldsymbol{\ell}_{\mathrm{S}})\mathrm{d}\mathbf{x}$ the inertia tensor expressed in the inertial frame. When expressed in the body frame $\hat{\mathbf{I}}_{\mathrm{S}}$ becomes a constant diagonal tensor. The torques are expressed in the body frame as $\hat{\mathbf{T}} = \mathbf{R}_{\mathrm{S}}^{\top}\cdot\mathbf{T}$. The same transformation applies to the rotational velocity. The hydrodynamic force and torque are derived by assuming a momentum conservation between the solid assembly and the fluid. Since the capillary contribution is accounted for in the calculation of the intermediate velocity the two

	ξ/Δ	ξ_A^2/ξ^2	ξ_B^2/ξ^2	χ	r_b/Δ	ξ_b/Δ	ξ_c/ξ_b	Pe	Re	Ca	Bo	N	N_b
S1	-	-	-	-	6	3	[0.5,0.6]	-	0.01	-	-	128^3	[1-9]
S2	1	1	1	2.5	6	3	0.6	0.1	0.01	0.1	0	128^3	[25,24,24]
S3	1	[1,1.5]	[1,1.5]	2.5	[12.1,6,6]	3	0.6	0.1	0.01	1	[0.04-2.62]	$64 \times 128 \times 64$	[1,9,9]

TABLE I. Parameters used in the simulation sets S1, S2, and S3. The quantities with a length dimension are normalised with the size Δ of a grid element. N is the total number of grid nodes.

time integrals are given by

$$\int_{t^n}^{t^{n+1}} (\mathbf{F}_h + \mathbf{F}_c)\,\mathrm{d}t = \int_{\mathcal{V}} \rho\phi_S^{n+1}(\mathbf{u}^* - \mathbf{u}_S^*)\mathrm{d}\mathbf{x}, \quad (18)$$

$$\int_{t^n}^{t^{n+1}} (\mathbf{T}_h + \mathbf{T}_c)\,\mathrm{d}t = \int_{\mathcal{V}} \boldsymbol{\ell}_S^{n+1} \times \Big[\rho\phi_S^{n+1}(\mathbf{u}^* - \mathbf{u}_S^*)\Big]\mathrm{d}\mathbf{x}, \quad (19)$$

where $\mathbf{u}_S^* = \mathbf{V}_S^n + \boldsymbol{\Omega}_S^n \times \boldsymbol{\ell}_S^{n+1}$. Finally the velocity field of the assembly is enforced onto the total fluid velocity field as

$$\mathbf{u}^{n+1} = \mathbf{u}^* + \int_{t^n}^{t^{n+1}} \left(-\frac{1}{\rho}\nabla p_S + \phi_S \mathbf{f}_S\right)\mathrm{d}t. \quad (20)$$

The pressure p_S, originating from the rigidity constraint of the solid assembly, is obtained from the incompressibility condition $\nabla \cdot \mathbf{u}^{n+1} = 0$. The time integral of the force density field is calculated as

$$\int_{t^n}^{t^{n+1}} \phi_S \mathbf{f}_S \mathrm{d}t = \phi_S^{n+1}(\mathbf{u}_S^{n+1} - \mathbf{u}^*). \quad (21)$$

where $\mathbf{u}_S^{n+1} = \mathbf{V}_S^{n+1} + \boldsymbol{\Omega}_S^{n+1} \times \boldsymbol{\ell}_S^{n+1}$. The above equations are discretised in space using a second-order central differencing scheme for the first partial derivatives and a fifth-order compact scheme [21] for the second partial derivatives. The variables are advanced in time using a forward Euler method. The authors are aware of more efficient discretisation schemes [4, 22] normally employed for solving the advection Equation 7. It was however found that the above schemes delivered stable simulations when the capillary number exceeded Ca > 0.1. A mineral particle of about 100 µm in size and sedimenting in water towards an air-liquid interface normally attains a speed of some milometers per second [2]. Under such experimental conditions the capillary number typically falls below the value $\mathrm{Ca} < 10^{-3}$.

IV. RESULTS

The three dimensional grid is uniform. Because a Fast Fourier Transform is employed to solve the two discrete Poisson equations $\nabla \cdot \mathbf{u}^* = 0$ and $\nabla \cdot \mathbf{u}^{n+1} = 0$ periodicity is enforced on each side of the computational domain. A wall boundary could have been implemented using for instance a Neumann boundary condition [10]. The periodicity will rather affect the velocity field. It will have little adverse effect on the capillary force, since this force is computed across the diffuse colloidal interface. It is also assumed that the two fluids have equal viscosity and density. This assumption greatly simplifies the numerical modelling and will not alter the main message of this work, which is the development of a numerical model for simulating the dynamics of an arbitrarily shaped particle at a fluidic interface. The governing equations were implemented in their non-dimensional form using the Reynolds number Re, the Peclet number Pe, and the capillary number Ca given by

$$\mathrm{Re} = \frac{\rho U_0 L_0}{\eta},\ \mathrm{Pe} = \frac{U_0 L_0}{D_0},\ \mathrm{Ca} = \frac{\eta U_0}{\gamma_0}, \quad (22)$$

where U_0 is a reference velocity arbitrarily set. It could for instance be the terminal velocity of the solid assembly. The reference length is defined as $L_0 = \xi$, the diffusion coefficient as $D_0 = \mu_0 M$, and the reference surface tension as $\gamma_0 = \mu_0 L_0$. This non-dimensionalisation is identical to that used by other authors who previously simulated the phase separation of binary fluids [23, 24]. The simulation parameters of all the subsequent simulations are summarised in Table I.

A. Drag force acting on a solid assembly (S1)

The hydrodynamic validation of the smooth profile method has previously been performed [10, 16]. However to ensure the correctness of our in-house implementation, the settling of a bead chain in a monophasic fluid is first simulated. In the present simulations (S1), the sharp boundaries of two successive beads do not overlap, i.e. $|\mathbf{X}_b - \mathbf{X}_{b-1}| = 2r_b$. The bead chain, subject to a constant external force, is initially placed at the centre of the system and eventually reaches its terminal velocity after a short period of time. The terminal velocity of the chain relative to the fluid is calculated as

$$\mathbf{V}_S^\infty - \mathbf{V}_f = \mathbf{V}_S^\infty - \frac{\int_{\mathcal{V}} \mathbf{u}\mathrm{d}\mathbf{x}}{\int_{\mathcal{V}} \mathrm{d}\mathbf{x}}. \quad (23)$$

The open source program HYDROLIB [25], which achieves an accuracy in the Stokes drag below 1%, is used

for the calculation of the reference values. Because of the periodicity enforced on each side of the domain the normalised theoretical terminal velocity of a single bead does not equal unity but $\widetilde{\mathrm{V}}_{\mathrm{S}}^{\infty} = 1 - 1.7601c^{1/3} + c - 1.5593c^2$, where $c = 4\pi \mathrm{r}_b^3/(3L^3)$ [26, 27]. The theory delivers a value of $\widetilde{\mathrm{V}}_{\mathrm{S}}^{\infty} = 0.87$, HYDROLIB [25] a value of $\widetilde{\mathrm{V}}_{\mathrm{S}}^{\infty} = 0.87$ and the present simulation a value of $\widetilde{\mathrm{V}}_{\mathrm{S}}^{\infty} = 0.76$. The non-dimensionalised relative terminal velocity is shown in Figure 2. The figure also illustrates

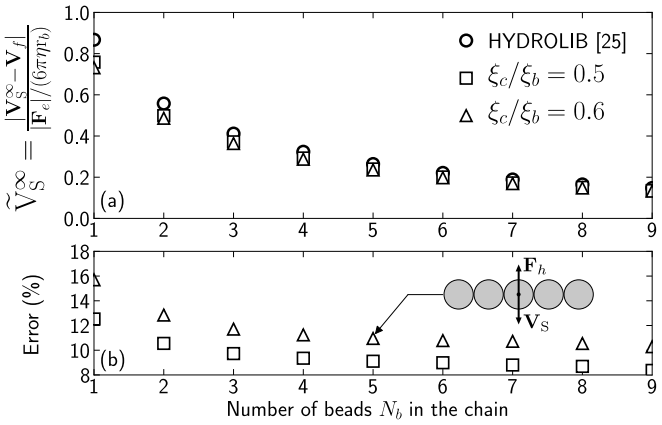

FIG. 2. Relative terminal velocity as a function of the number of beads in the three dimensional chain (Top). The reference data obtained with the open-source program HYDRLIB [25] are used to calculate the relative errors (Bottom).

the relative terminal velocity with increasing number of beads for two cut-off lengths ξ_c (See Equation 1). The relative error decreases with the number of beads. In the case of the sphere and of the short rods ($N_b \leq 3$) the larger errors can probably be attributed to the contribution of the relatively inaccurate flow field around both rod extremities. The longer the rod is, the smaller is the contribution of its extremity on the total drag. With a larger number of beads in the chain both the error and the terminal velocity eventually reach constant values. With an interfacial thickness set to $\xi_b/\Delta = 3$ and a bead radius set to $\mathrm{r}_b/\Delta = 6$ an accuracy of 11% and 9%, respectively, in the terminal velocity are achieved for $\xi_c/\xi_b = 0.5$ and $\xi_c/\xi_b = 0.6$. This error range is in line with previously reported data [15, 16]. A smaller value of ξ_b results in more accurate results. A smaller interfacial thickness is however associated with a higher grid resolution and a smaller time increment. We therefore choose for all subsequent simulations since it achieves an efficient trade-off between accuracy and numerical efficiency.

B. Solid assembly at a fluidic interface (S2)

The rotational motion of various arbitrary geometries at a fluidic interface is presently tested. As illustrated in Figure 3 (set S2) the dynamics of a ring-like, of a rod-like, and of a plate-like assembly are simulated. The three assemblies have almost equal mass and are not subject to an external force. The distance from the centre of mass of the b-th bead to the nearest neighbouring bead is set to $|\mathbf{X}_b - \mathbf{X}_b^{\mathrm{nearest}}| = 2(\mathrm{r}_b - \xi_c)$. The fluidic interface, defined as the isosurface $\psi(\mathbf{x}) = 0$ forms a horizontal plane at the time $t/t_0 = 0$, where $t_0 = L_0/U_0$. The centre of mass of each assembly coincides with the fluidic interface initially at rest. The orientation angle α between the long axis and the fluidic interface is arbitrarily set to $\alpha = 75°$. This slight inclination is imposed to avoid the unstable upright position at $\alpha = 90°$. Figure 4 shows that, as a result of the capillary torque, each solid assembly smoothly rotates about the $\hat{\boldsymbol{y}}$-axis until a stable position is reached. The lack of available data on the rotational motion of elongated particles at a fluidic interface makes it impossible to quantitatively compare the evolution of the angular position. The present simulations hence act as qualitative tests and allow us to verify the final orientation of the solid assembly attained at the equilibrium. As expected the long axis $\hat{\mathbf{x}}$ of each solid assembly eventually aligns with the fluidic interface. The slower rotation of the ring and of the rod can be partly explained by looking at the respective ratios of momentum inertias. The two inertia ratios $\hat{\mathrm{I}}_{yy}^{\mathrm{ring}}/\hat{\mathrm{I}}_{yy}^{\mathrm{plate}} = 3.22$ and $\hat{\mathrm{I}}_{yy}^{\mathrm{rod}}/\hat{\mathrm{I}}_{yy}^{\mathrm{plate}} = 5.17$ cause the plate to reach a stable equilibrium more rapidly. The plate reaches an orientation angle close to $\alpha \approx 4°$. Further simulations showed that a smaller ratio of the fluidic interfacial thickness to the bead radius ξ/r_b brought the inclination angle to zero.

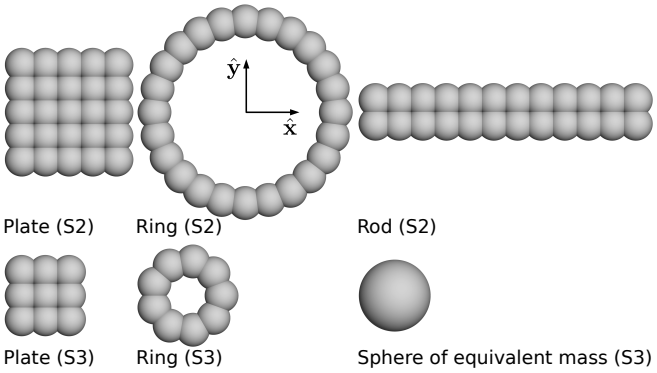

FIG. 3. Three-dimensional solid assemblies used in the two simulation sets S2 and S3.

C. Solid assembly crossing a fluidic interface (S3)

The settling of three solid assemblies across a fluidic interface is now investigated. The size of the domain and the number of beads in each assembly are reduced to save computational time. The rod-like geometry is left out and replaced with a sphere of equivalent mass (See Figure 3). Each assembly is subject to a constant external force which pulls the assembly in the downward

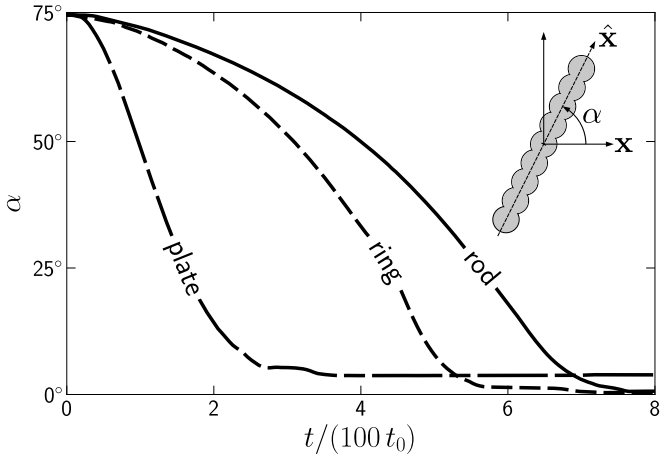

FIG. 4. Orientation α of each solid assembly as a function of time. At the time $t/t_0 = 0$ the centre of mass is placed at the fluidic interface initially set in horizontal position.

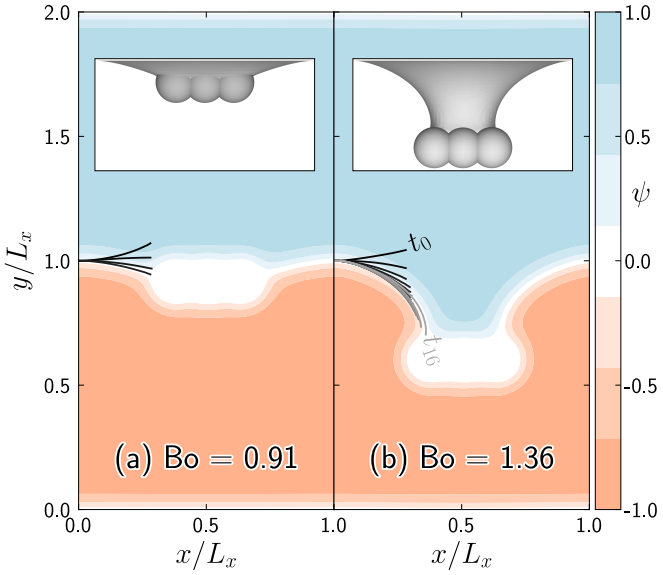

FIG. 5. Evolution of the fluidic interface for various Bond numbers. The time step between two successive isolines coloured in grey is constant. The 3D plots and the field mid-sections ψ are shown for the plate (S3) at time t_3 and t_{16} respectively.

vertical direction. The sagittal plane of each assembly is set in position normal to the external force. The centre of mass of each solid assembly is initially placed at the altitude $\mathrm{Y_S}(0)/\mathrm{r}_b^{\mathrm{eqv}} = 2.15$ relative to the horizontal fluidic interface initially at rest. The term "eqv" hereafter indicates a quantity associated with the sphere of equivalent mass. This altitude was found large enough for each solid assembly to reach its terminal velocity before being affected by the capillary force. The temporal deformation of the fluidic interface is shown in Figure 5 for two Bond number numbers. In the left subfigure the plate gets trapped at the interface (Bo=0.91). In the right subfigure the plate later detaches (Bo=1.36). See the Supplemental Material [28] for a video clip of the simulation. The Bond number indicates the ratio of the downward force to the reference capillary force. The formulation previously used by other authors [29, 30] for a spherical colloidal particle is here retained for comparison purposes. The Bond number, rewritten as a function of the external force $\mathbf{F}_e$, is given by

$$\mathrm{Bo} = \frac{(\rho_\mathrm{S} - \rho)\, g\, \mathrm{r}_{\mathrm{eqv}}^2}{\gamma_{\mathrm{AB}}} = \frac{3|\mathbf{F}_e|}{4\pi\gamma_{\mathrm{AB}}\mathrm{r}_{\mathrm{eqv}}} \tag{24}$$

where g is the gravitational acceleration and γ_{AB} the fluidic surface tension. In the absence of a solid phase a fourth-order expansion of Equation 6 will show that the free energy takes the form $f(\psi, 0) = -\alpha\psi^2/2 + \beta\psi^4/4 + \kappa|\nabla\psi|^2/2$, where $\alpha = \chi/2 - 1$, $\beta = 1/3$, and $\kappa = \xi^2 + (\xi_\mathrm{A}^2 + \xi_\mathrm{B}^2)/4$ [14]. The fluidic surface tension is then given by [13, 31]

$$\gamma_{\mathrm{AB}} = \mu_0 \frac{(2\alpha)^{3/2}\kappa^{1/2}}{3\beta}. \tag{25}$$

Previous experiments have shown that for $\mathrm{Bo} \ll 1$ the fluidic interface is able to sustain the solid assembly with little deformation. With increasing Bo, the assembly penetrates deeper into the bottom fluid phase, resulting in a larger deformation of the fluidic interface. Figure 6 shows the relative vertical displacement $h/\mathrm{r}_{\mathrm{eqv}}$ as a function of the Bond number for three different contact angles θ. The interfacial energy, and thus the contact angle, is set by changing the two Cahn coefficients ξ_A/ξ and ξ_B/ξ. The persisting spurious velocities, known to appear near curved diffuse interfaces and previously reported by others [4, 32], affect the curvature of the fluidic interface in the vicinity of the assembly. For $\theta \neq 90°$ the fluidic interface is slightly curved near the three-phase contact line because of these spurious currents. Therefore, equation 7 is solved independently for an exact estimation of the contact angle. The procedure used to compute and set the contact angle is explained in detail in our previous work [14]. For a spherical particle with a contact angle $\theta = 90°$, i.e. for a particle with equal affinity for the two fluids, the agreement between the present numerical results and those taken from the work of Stratford *et al.* [29] is generally good. For comparison purposes a second set of data, taken from the work of Davies *et al.* [5], is also shown. Table II lists the critical Bond numbers at which the three assemblies break away from the fluidic interface. A spherical particle with a contact an-

θ	Sphere (Theory)	Sphere [5]	Sphere	Plate	Ring
64°	-	0.25	0.25	0.57	0.57
90°	0.75	0.45	0.68	1.25	1.37
116°	-	0.60	1.37	2.28	2.62

TABLE II. Critical Bond numbers at which particle detachment off the fluidic interface occurs.

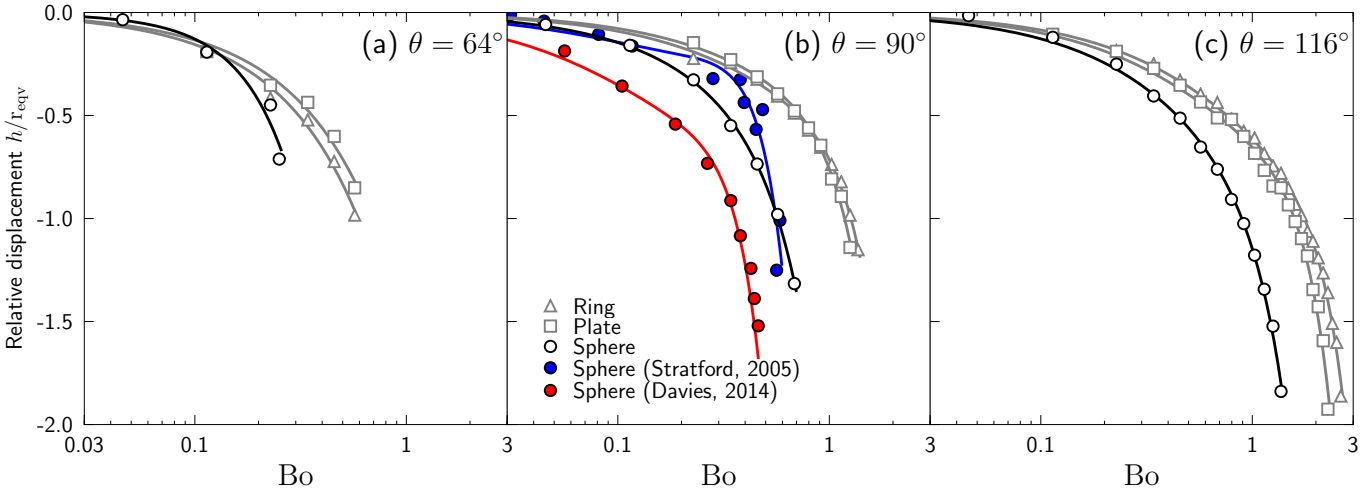

FIG. 6. Relative vertical displacement of the assembly in the bottom fluid as a function of the Bond number. Data associated with a detachment are not shown.

gle $\theta = 90°$ theoretically detaches at the critical value Bo = 0.75 [29, 30]. The critical Bond number Bo, here estimated at Bo = 0.68, matches well this theoretical value. Table II shows that the plate detaches at a critical Bond number Bo = 1.25 and the ring at an even greater critical Bond number Bo = 1.37. In the case of the ring a first three-phase contact line lies on the inner part of the geometry and a second line on the outer part. These two contact lines quantitatively explains why the ring is harder to dislodge. Results of this study also show that, irrespective of the geometry, the critical Bond number increases with the contact angle. The numerical data of Davies *et al.* [5] corroborate qualitatively this finding, even though the discrepancies tend to increase with larger contact angles. The detachment process is further illustrated in Figure 7. The velocity of the three solid assemblies is shown as a function of the altitude Y_S of the centre of mass. For the lowest Bond number attachment occurs in all cases and the Lagrangian velocity of the assemblies drops to zero. With increasing Bond number the detachment eventually occurs. For Bo = 1.82 the velocity of the sphere is nearly unperturbed by the capillary force.

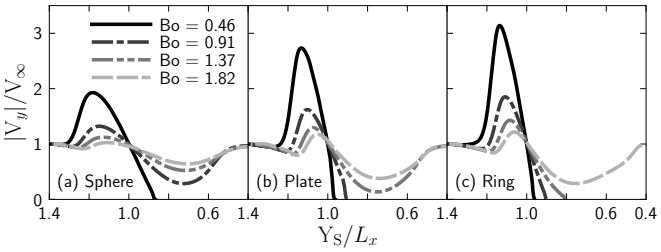

FIG. 7. Vertical velocity component V_y as a function of the particle altitude, where $(V_x\, V_y\, V_z)^\top = \mathbf{V}_S$. The data are shown for $\theta = 90°$.

V. CONCLUSIONS

The present three-phase model, previously developed for a single sphere [14], was further improved to simulate the dynamics of arbitrarily shaped colloidal particles in a binary fluid. The method, based on the decomposition of a particle into a collection of beads, is relatively straightforward to implement and allows for intricate three-dimensional shapes to be studied numerically. The hydrodynamic performance of the model was validated and showed a precision of about 10% (S1). The dynamics of a rod-like, of a plate-like, and of a ring-like particle at a fluidic interface were then tested. It was found that plate-like particles attach more rapidly to a fluidic interface (S2) and are subsequently harder to dislodge (S3). The theoretical critical Bond number Bo, at which a spherical particle with equal affinity for the two fluids breaks away from a fluidic interface, equals Bo = 0.75. This value is in line with our numerical experiments. A plate and a ring of equivalent masses were found to detach at greater critical Bond numbers, approximately equal to Bo = 1.3. The results of this study will find application in the stabilisation of emulsions and in the recovery of mineral particles by rising bubbles. In both applications the stability of the particle-bubble aggregate will be affected by the particle shape. Future extension of this work will include the study of multiparticle systems in binary flows. Decomposing the arbitrarily shaped colloids into a series of beads will certainly prove beneficial for an effective simulation of the interparticle interactions.

ACKNOWLEDGMENTS

This work was supported by a Marie Curie International Outgoing Fellowship with the European Union

Seventh Framework Program for Research and Technological Development (2007-2013) under the grant agreement number 623518.

[1] F. Jansen and J. Harting, Phys. Rev. E **83**, 046707 (2011).
[2] G. Lecrivain, G. Petrucci, M. Rudolph, U. Hampel, and R. Yamamoto, Int. J. Multiphase Flow **71**, 83 (2015).
[3] A. Joshi and Y. Sun, Phys. Rev. E **79**, 066703 (2009).
[4] M. Fujita, O. Koike, and Y. Yamaguchi, J. Comput. Phys. **281**, 421 (2015).
[5] G. Davies, T. Kruger, P. Coveney, J. Harting, and F. Bresme, Soft Matter **10**, 6742 (2014).
[6] G. Davies, T. Kruger, P. Coveney, and J. Harting, J. Chem. Phys. **141**, 154902 (2014).
[7] X. Luu and A. Striolo, J. Phys. Chem. B **118**, 13737 (2014).
[8] P. Millett and Y. Wang, J. Colloid Interface Sci. **353**, 46 (2011).
[9] T. Cheng and Y. Wang, J. Colloid Interface Sci. **402**, 267 (2013).
[10] X. Luo, M. Maxey, and G. Karniadakis, J. Comput. Phys. **228**, 1750 (2009).
[11] S. Yamamoto and T. Matsuoka, J. Chem. Phys. **98**, 644 (1993).
[12] T. Araki and H. Tanaka, Phys. Rev. E **73**, 061506 (2006).
[13] H. Shinto, Adv. Powder. Technol. **23**, 538 (2012).
[14] G. Lecrivain, R. Yamamoto, U. Hampel, and T. Taniguchi, Phys. Fluids **28**, 083301 (2016).
[15] Y. Nakayama and R. Yamamoto, Phys. Rev. E **71**, 036707 (2005).
[16] J. Molina and R. Yamamoto, J. Chem. Phys. **139**, 1 (2013).
[17] Y. Nakayama, K. Kim, and R. Yamamoto, Eur. Phys. J. E **26**, 361 (2008).
[18] J. Molina, K. Otomura, H. Shiba, H. Kobayashi, M. Sano, and R. Yamamoto, J. Fluid Mech. **792**, 590 (2016).
[19] N. Oyama, J. Molina, and R. Yamamoto, Phys. Rev. E **93**, 043114 (2016).
[20] G. Lecrivain, R. Rayan, A. Hurtado, and U. Hampel, Comput. Fluids **124**, 78 (2016).
[21] W. Spotz and G. Carey, Numer. Methods Partial. Differ. Equ. **12**, 235 (1996).
[22] H. Ding, P. Spelt, and C. Shu, J. Comput. Phys. **226**, 2078 (2007).
[23] R. Chella and J. Vinals, Phys. Rev. E **53**, 3832 (1996).
[24] V. Badalassi, H. Ceniceros, and S. Banerjee, J. Comput. Phys. **190**, 371 (2003).
[25] K. Hinsen, Comput. Phys. Commun. **88**, 327 (1995).
[26] H. Hasimoto, J. Fluid Mech. **5**, 317 (1959).
[27] A. Sangani and A. Acrivos, Int. J. Multiphase Flow **8**, 343 (1982).
[28] "URL will be inserted by publisher,".
[29] K. Stratford, R. Adhikari, I. Pagonabarraga, and J. C. Desplat, J. Stat. Phys. **121**, 163 (2005).
[30] J. Onishi, A. Kawasaki, Y. Chen, and H. Ohashi, Comput. Math. Appl. **55**, 1541 (2008).
[31] D. Anderson, G. McFadden, and A. Wheeler, Annu. Rev. Fluid Mech. **30**, 139 (1998).
[32] C. Pooley and K. Furtado, Phys. Rev. E **77**, 046702 (2008).